Multiseasonal Predictions with a Coupled Tropical Ocean–Global Atmosphere System

BEN P. KIRTMAN, J. SHUKLA, BOHUA HUANG, ZHENGXIN ZHU, AND EDWIN K. SCHNEIDER

Center for Ocean–Land–Atmosphere Studies, Institute of Global Environment and Society, Inc., Calverton, Maryland

(Manuscript received 18 May 1995, in final form 30 November 1995)

ABSTRACT

The Center for Ocean–Land–Atmosphere Studies anomaly coupled prediction system, using a sophisticated dynamical model of the tropical Pacific Ocean and the global atmosphere, is described. The resolution of the component models is moderate, with the atmospheric spectral model truncated at triangular total wavenumber 30 and 18 vertical levels. The ocean model is a Pacific Basin model with 0.5° latitude and 1.5° longitude resolution in the waveguide and 20 vertical levels. The performance of the uncoupled component models motivates the anomaly coupling strategy and has led to the development of a simple empirical technique for converting the 850-mb zonal wind into a zonal surface stress that is used in the prediction experiments described here. In developing ocean initial conditions, an iterative procedure that assimilates the zonal wind stress based on the simulated sea surface temperature anomaly error is applied. Based on a sample of 78 18-month hindcasts, the predictions have useful skill in the Nino-3 region for at least 12 months. The systematic error of the predictions is shown to be relatively small because the ocean initial conditions are in reasonable equilibrium with the ocean model. Finally, composites of the hindcast warm El Niño–Southern Oscillation (ENSO) events indicate that the model simulates the basic features of ENSO, but there are errors in the horizontal structure of the sea surface temperature anomaly that potentially limit the predictability of the model.

1. Introduction

The most well-known interaction between the atmosphere and the ocean is the large interannual variation in sea surface temperature, circulation, and rainfall in the tropical Pacific. It is now commonly understood that this interannual variation is a manifestation of a coupled ocean–atmosphere instability that is referred to as El Niño and the Southern Oscillation (ENSO; Philander 1990), and it offers the greatest potential for useful seasonal to interannual climate predictions. In recent years, there have been a number of attempts to capitalize on the predictability of ENSO with different statistical and dynamical models (Cane and Zebiak 1985, 1987; Cane et al. 1986; Leetmaa and Ji 1989; Ji et al. 1994; Balmaseda et al. 1994; Barnston and Ropelewski 1992; Kleeman 1993; Barnett et al. 1993, 1994; among others). The various forecasting methods fall into four categories, one of which is purely statistical. The remaining three methods are either purely dynamical or are a combination of dynamical and statistical methods. The intermediate coupled model (ICM) approach is dynamically based and uses simplified models of the ocean and atmosphere (Cane et al. 1986; Zebiak and Cane 1987; Kleeman 1993; among others). The hybrid coupled models (HCM) generally use ocean general circulation models (OGCM) and either a simplified dynamical or statistical atmosphere model (Neelin 1990; Latif and Villwock 1990; Jin and Neelin 1993; Barnett et al. 1993; Graham and Barnett 1995). The coupled general circulation model approach (CGCM) uses a dynamical OGCM and an atmospheric general circulation model (AGCM). The CGCM method of seasonal to interannual climate predictions is advanced in this paper and a CGCM strategy is also used for operational prediction at the National Centers for Environmental Prediction (NCEP, formerly known as the National Meteorological Center) (Ji et al. 1994). Latif et al. (1994) provide a comprehensive review of ENSO prediction studies.

The ICM approach was pioneered by Cane et al. (1986) and Zebiak and Cane (1987) and is used to produce ENSO forecasts operationally. The forecast system used in Zebiak and Cane (1987), hereafter referred to as ZC, uses a simple Gill-type (1980) atmosphere and a one active layer ocean model. Over all initial times, the eastern equatorial Pacific sea surface temperature anomaly (SSTA) forecasts were skillful out to a year, but there was also substantial dependence of forecast skill on the initial time of the forecast. Forecasts initialized in January had the shortest predictive lead time, while those initialized in April had the longest useful lead. More recently, Chen et al. (1995) have introduced an initialization procedure to the ZC coupled system that dramatically improves the eastern equatorial Pacific

Corresponding author address: Dr. Ben P. Kirtman, Center for Ocean–Land–Atmosphere Studies, Institute of Global Environment and Society, Inc., 4041 Powdermill Road, Suite 302, Calverton, MD 20705-3106.
E-mail: kirtman@cola.iges.org

SSTA forecasts, particularly for predictions initialized during the 1980s. However, during more recent events, the predictive skill is not much different from the ZC system without the new initialization (S. Zebiak 1995, personal communication). In the results of Chen et al. (1995) the sensitive dependence of forecast skill on initial time was eliminated. A ZC-type model has also been used by Kleeman (1993) and Kleeman et al. (1995) for forecasting and data assimilation experiments. The ICM method has also been employed to study the predictability of the coupled system (Goswami and Shukla 1991a,b; Blumenthal 1991; Jin et al. 1994).

The HCM approach has been used in a number of mechanistic studies (Neelin 1990; Latif and Villwock 1990; Jin and Neelin 1993; Neelin and Jin 1993) and in prediction studies (Barnett et al. 1993; Graham and Barnett 1995; Barnett et al. 1994). The motivation behind the HCM is that the predictive memory of the coupled system lies in the ocean thermal structure and the atmospheric response is in equilibrium with the ocean. Therefore, the HCM system focuses on the evolution of the ocean, and the atmosphere is treated as a rapidly adjusting component of the coupled system.

The CGCM approach has received considerable attention in mechanistic and simulation studies (Philander et al. 1992; Latif et al. 1993a,b; Mechoso et al. 1995; among others). In the prediction mode, there have only been a few attempts (Latif et al. 1993b; K. Miyakoda 1995, personal communication; Leetmaa and Ji 1989; Ji et al. 1994). The NCEP effort (Leetmaa and Ji 1989; Ji et al. 1994), like the Geophysical Fluid Dynamics Laboratory (GFDL) effort (K. Miyakoda 1995, personal communication), includes a sophisticated ocean data assimilation system to initialize the forecasts (Ji et al. 1995, 1996). In a pilot project at the Center for Ocean–Land–Atmosphere Studies (COLA), Zhu and Schneider (1995) considered the anomaly coupled CGCM approach. The prediction model is considered anomaly coupled because the component models predict the total field, but the coupling procedure is to exchange only the predicted anomalies plus a prescribed climatology at the interface of the ocean and the atmosphere model. The atmosphere and ocean components of the coupled model presented here are similar to those used at NCEP; however, the coupling strategy and the development of ocean initial conditions differ substantially. While the prediction system presented here primarily falls in the CGCM category, the anomaly coupling strategy, the empirical corrections to the zonal wind stress, and the iterative initialization procedure discussed here indicate the influence that the HCM and ICM approaches have on the current CGCM prediction efforts.

The focus of the work presented here is threefold. First, we describe the anomaly coupled prediction system and its performance with an ensemble of 78 hindcast experiments. It is shown that the anomaly coupled model produces SSTA hindcasts in the tropical eastern Pacific that are well correlated with the observed SSTA for lead times of up to one year in advance. Composites of the hindcast ENSO events indicate that the model simulates the basic features of ENSO but that the meridional scale of the hindcast SSTA is too small, which potentially limits the predictability of the model.

Second, we demonstrate that empirical constraints on the AGCM zonal wind stress improves uncoupled simulations and coupled hindcasts. The empirical formulation for the AGCM zonal wind stress is described in more detail in Huang and Shukla (1997) and is motivated by errors in the AGCM boundary layer, which produces zonal wind stress anomalies that are far too confined to the western extreme of the Pacific basin. These zonal wind stress errors are circumvented by using the AGCM zonal winds at the top of the boundary layer (approximately 850 mb) to empirically redefine the zonal surface stress. Similar problems with the zonal wind stress were also found at NCEP, and they also apply empirical corrections to the zonal wind stress (M. Ji 1995, personal communication). These various statistical corrections to the zonal wind stress anomalies indicate the influence of the HCM approach, such as in Barnett et al. (1993), on the CGCM approach.

Third, we describe an iterative ocean initialization procedure that modifies the zonal wind stress anomaly based on the simulated SSTA error. The motivation for the initialization is to improve the ocean initial state for coupled predictions without assimilating subsurface or satellite data. The details of the iteration are discussed in Kirtman and Schneider (1996), and we show here that this initialization improves the hindcast skill. Chen et al. (1995) have also found substantial improvements in forecast skill with their initialization procedure, which shows that the ICMs potentially identify strategies and methods for improving CGCM forecasts.

The remainder of this paper is as follows. Section 2 describes the component atmosphere and ocean models. Section 3 discusses the coupling strategy and how the AGCM 850-mb zonal winds are empirically converted into a zonal wind stress in the prediction experiments. The development of initial conditions is based on an iterative procedure that is presented in section 4. The 78 18-month predictions and their systematic errors and skill are described in section 5. Section 6 presents predicted warm ENSO composites. Finally, section 7 contains a summary and some concluding remarks.

2. The component models

The ocean and atmosphere models used in this study are described below. The atmospheric model has been used in a number of ENSO related predictability studies (Fennessy et al. 1994; Fennessy and Shukla 1991). The ocean model has also been used for ENSO studies and has been shown to give reasonable interannual variability (Schneider et al. 1997; Huang and Schneider 1995; Kirtman and Schneider 1996).

a. The ocean model

The ocean model used in this study is a Pacific basin model adapted from the GFDL modular ocean model (Bryan and Lewis 1979; Rosati and Miyakoda 1988; Pacanowski et al. 1993) and throughout this paper will be referred to as the GFDL ocean model. This model is a finite difference treatment of the primitive equations of motion using the Boussinesq and hydrostatic approximations in spherical coordinates. The model includes nonlinear vertical mixing of heat, salinity, and momentum that is Richardson number dependent (Pacanowski and Philander 1981), and horizontal mixing of momentum. The domain of the ocean model is restricted to the Pacific basin (30°S–45°N, 130°E–80°W). The zonal resolution is 1.5° and, in the deep Tropics (10°S–10°N), the meridional resolution is 0.5°, linearly increasing to 1.5° at 20°S and 20°N. Beyond 20°S and 20°N the meridional resolution is 1.5°. There are 20 vertical levels to a maximum depth of 4000 m and the top 16 levels are between 0 and 400 m. This configuration of the model and the formulation of the heat and salinity fluxes is the same as that used by Huang and Schneider (1995) and Kirtman and Schneider (1996). The horizontal diffusion coefficient is taken to be 2×10^7 cm^2 s^{-1}.

One of the limitations of the forced ocean model experiments and the coupled prediction experiments presented here is in the heat flux formulation. It is fairly well known that this heat flux formulation acts as a damping or relaxation of the simulated SSTA (Schneider et al. 1995). Therefore, since both the prediction experiments and the uncoupled ocean experiments use this simple parameterized formulation of the heat flux, the bulk of the SSTA variability is due to the wind stress alone.

The observed wind stress forcing used here was constructed from the Florida State University (FSU) pseudostress. The data come from analyzing tropical Pacific ship and station measurements and are subjectively analyzed to a $2° \times 2°$ grid as described in Goldenberg and O'Brien (1981). The pseudostress was converted to a wind stress by assuming a constant air density of 1.25×10^{-3} g cm^{-3} and a drag coefficient based on the formulation of Trenberth et al. (1990). The data available are for monthly means from January 1964 to September 1994.

b. The atmospheric model

The atmospheric model used in the experiments described here is the COLA AGCM. Only a very brief description of the AGCM is provided here. More details can be found in Schneider and Kinter (1994), Xue et al. (1991), and Kinter et al. (1988). The model is a global spectral model with triangular truncation at wavenumber 30. There are 18 unevenly spaced σ coordinate vertical levels. The model includes the simplified biosphere model over land described in Xue et al. (1991); the parameterization of the solar radiation is after Lacis and Hansen (1974); and the terrestrial radiation follows Harshvardhan et al. (1987). The deep convection scheme incorporates a modified version of the Kuo (1965) scheme and the shallow convection follows Tiedtke (1984). There is a second-order turbulent closure scheme for subgrid-scale exchanges of heat, momentum, and moisture as in Miyakoda and Sirutis (1977) and Mellor and Yamada (1982) at their closure level 2.0. Surface wave drag and the vertical distribution of the wave drag due to vertically propagating gravity waves is parameterized following the procedure by Pierrehumbert (1987), Palmer et al. (1986), and Helfand et al. (1987) (see Kirtman et al. 1993 for details).

The AGCM experiments described here use prescribed SST after either Reynolds (1988) for the period 1982–94 or SST provided by C. K. Folland of the Hadley Centre for the period 1948–81. The SSTA for the entire record (1948–94) is computed as the deviation from the mean annual cycle computed separately for both SST datasets. In other words, there are different SST climatologies for the Reynolds (1988) data and the Hadley Centre data, and the SSTA is computed with respect to the appropriate climatology. The AGCM wind and wind stress data used in the following experiments come from an extended integration of the AGCM using the prescribed SST for 1948–94.

3. The coupling strategy

As mentioned earlier, we employ an anomaly coupling strategy. The ocean and atmosphere models exchange predicted anomalies, which are computed relative to their own model climatologies, while the climatology upon which the anomalies are superimposed is specified by observations. The model climatologies are defined by separate uncoupled extended simulations of the ocean and atmosphere models. In the case of the atmosphere, the model climatology is computed from a 45-yr (1949–94) integration with specified observed SST, and in the case of the ocean we use a 30-yr (1964–94) integration with prescribed FSU wind stress and parameterized heat flux as described in section 2.

In the prediction mode, the anomaly coupling strategy may be viewed as follows. Given an SST field, the AGCM predicts a wind stress field (τ). The AGCM wind stress climatology (τ_c), computed from the 45-yr uncoupled simulation described above, is then subtracted, and the anomaly ($\tau_a = \tau - \tau_c$) is added to the observed climatology (τ_o) so that the predicted total wind stress field (τ_p) used to force the ocean model is given by

$$\tau_p = \tau - \tau_c + \tau_o.$$

Given τ_p, the ocean model produces an SST field (T). The ocean model SST climatology (T_c), calculated from the 30-yr uncoupled simulation described above, is then

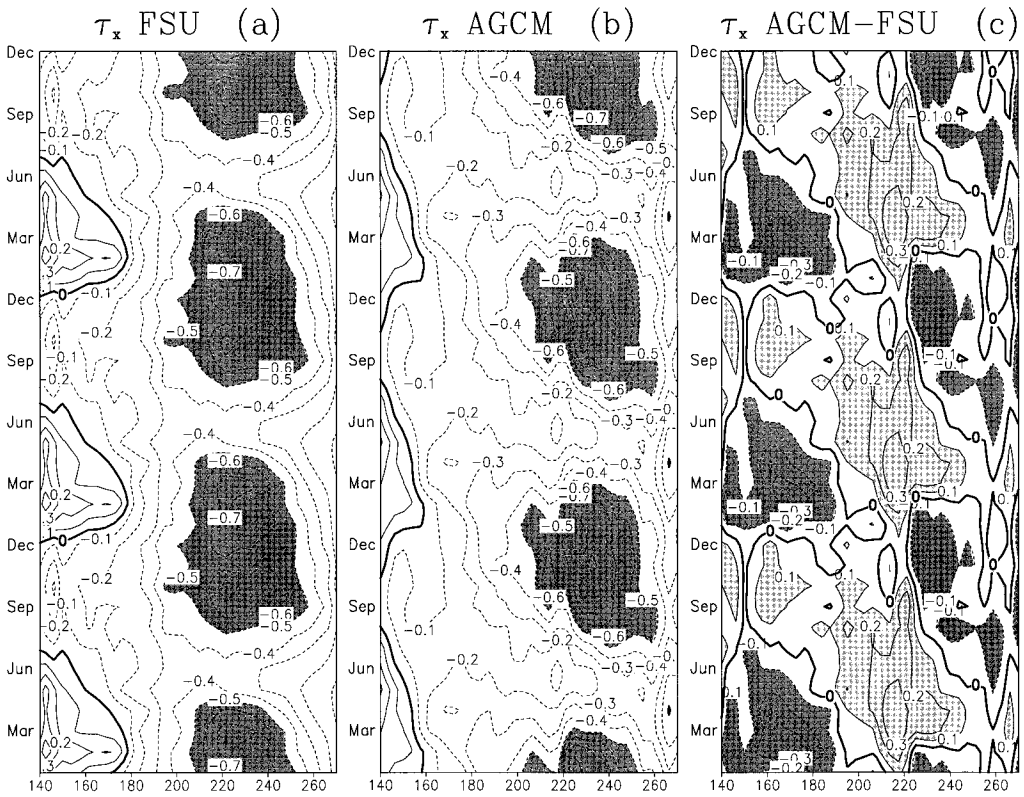

FIG. 1. Time–longitude cross section of the zonal wind stress annual cycle along the equator: (a) FSU annual cycle, (b) AGCM surface wind stress annual cycle, and (c) difference between AGCM and FSU data. Contour interval 0.1 dyn cm^{-2}.

subtracted and the observed climatology (T_o) is added so that the predicted total SST (T_p) is given by

$$T_p = T - T_c + T_o.$$

The observed wind stress climatology (τ_o) is computed from the 30 years of FSU wind stress data (1964–93) and the observed SST climatology (T_o) is calculated from the Reynolds (1988) blended analysis.

The ocean and atmosphere exchange information once per simulated day and a 30-day running mean is applied to both the wind stress anomaly and the SSTA. The running mean is applied during the hindcast using the current 24-h period and the previous 29 days. The formulation of the parameterized heat flux for both the ocean and atmosphere components of the coupled model is the same as in the uncoupled simulations.

The motivation for the anomaly coupling strategy is the errors found in the climatologies of uncoupled simulations of the ocean and atmosphere models. In addition, errors in the annual cycle that would affect ENSO predictions were noted in an extended integration of the directly coupled model (see Mechoso et al. 1995; Schneider et al. 1997). The anomaly coupling strategy also reduces the climate drift of the model.

Figure 1 shows three repeated annual cycles of zonal wind stress along the equator calculated from the 45-yr simulation of the uncoupled AGCM (τ_c). The FSU annual cycle (τ_o) and the error in the simulated annual cycle ($\tau_c - \tau_o$) are also shown in Fig. 1. The model captures the broad features of the annual cycle with easterlies throughout most of the equatorial Pacific. The simulated annual cycle of surface stress has an apparent spurious tendency for westward propagation much like the annual cycle in the observed SST (see Fig. 2). The annual cycle of the FSU data shows little propagation, suggesting that the AGCM wind stress may be too sensitive to the lower boundary condition of SST. In the error field, the westward propagation of the AGCM annual cycle is seen as westerly errors that have a maximum of 0.3 dyn cm^{-2} in the central Pacific during boreal spring that gradually move to the western Pacific in late summer to early fall. If full coupling were used, these errors would lead to warm ENSO-like conditions each boreal spring. In the western Pacific, the errors are largest in the boreal winter when the AGCM fails to capture the intensity of the westerlies. In the eastern Pacific, the errors tend to be somewhat smaller with the model having too much easterly momentum. By design, the anomaly coupling strategy removes the error in the annual cycle; however, as shown in the next section, additional modifications to the wind stress anomaly are required.

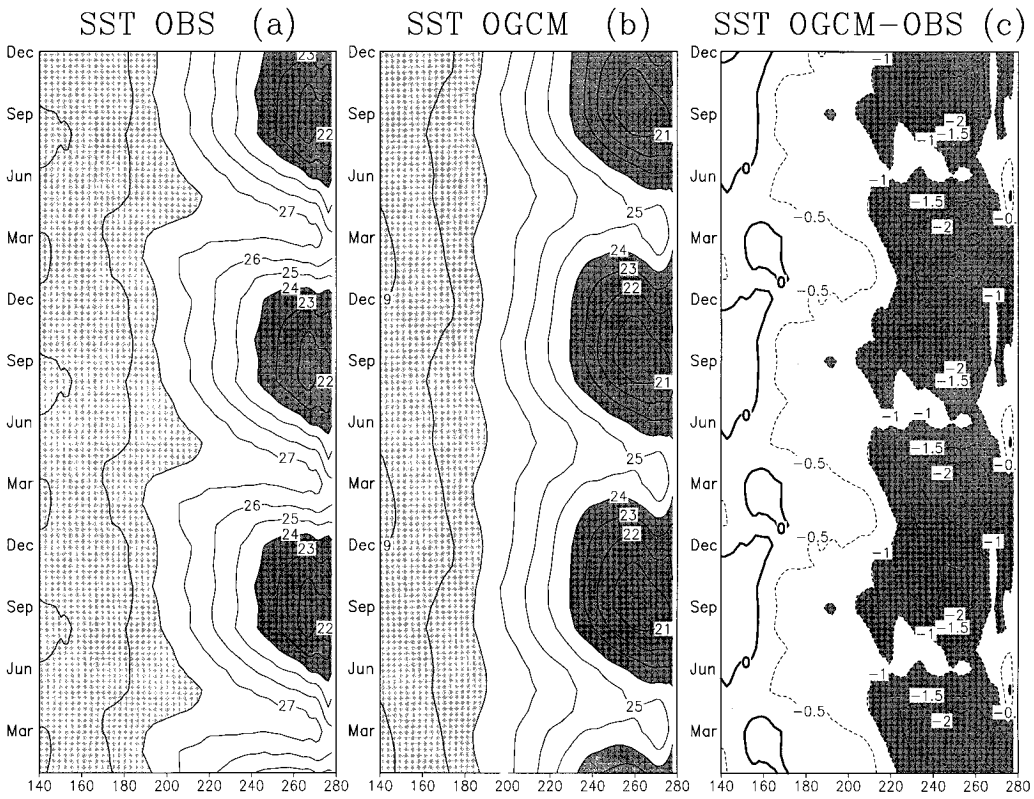

FIG. 2. Time–longitude cross section of the SST annual cycle along the equator: (a) Reynolds observed annual cycle, (b) OGCM annual cycle with FSU forcing, and (c) difference between OGCM and observed data.

Figure 2 shows the mean annual cycle of the SST along the equator as simulated by the OGCM with prescribed FSU wind stress forcing (T_c). The observed SST (T_o; Reynolds 1988) and the SST error ($T_c - T_o$) are also shown in Fig. 2. The OGCM captures the phase and, to some degree, the westward propagation of the annual cycle. Throughout most of the basin along the equator, the simulated annual cycle is colder than observed. The error is largest in the eastern Pacific where the SST is too cold by 2 K during most of the year.

While the general form of our coupling strategy is similar to that used by NCEP, there are some important differences in the details. For example, noting serious problems with the surface wind stress anomalies simulated by the AGCM, Ji et al. (1994) tuned the convective parameterization and the vertical diffusion. Similar problems with the COLA AGCM wind stress anomalies were noted by Huang and Schneider (1995) and Huang and Shukla (1997). Here, we have taken a different, and primarily empirical, approach to improving the momentum flux that was first discussed by Huang and Shukla (1997) and modified to include the annual cycle by Kirtman and Schneider (1996).

The problem with the simulated wind stress seems to be caused by errors in the boundary layer parameterization. This conjecture is based on the fact that relatively large temporal correlations are observed between the ECMWF zonal wind anomalies and the COLA AGCM zonal wind anomalies at 850 mb. On the other hand, the same correlation at the surface is quite low. Motivated by the high correlation at the top of the boundary layer, Huang and Shukla (1997) derived an empirical relation between the AGCM 850-mb zonal wind and the zonal surface stress. Kirtman and Schneider (1996) modified the Huang and Shukla (1997) formulation to include a longer record of observed data and the annual cycle. This empirical zonal wind stress formulation may be interpreted as an intermediate statistical model that includes dynamical constraints from the AGCM. The difference between this wind stress and those derived from statistical models, such as the one used in Barnett et al. (1993), is that it is explicitly constrained by the AGCM dynamics and physics. This approach also differs from that of Ji et al. (1994) in that they try to improve the simulation of surface stress by tuning the physical parameterizations, whereas we bypass the errors in the boundary layer by using the 850-mb zonal winds. Ultimately, the formulation of both the boundary layer and the convection in the model must be improved to make further progress in predicting the coupled ocean–atmosphere system.

With the prescription of the annual cycle of SST and wind stress from observations and the empirical corrections to the zonal wind stress based on the obser-

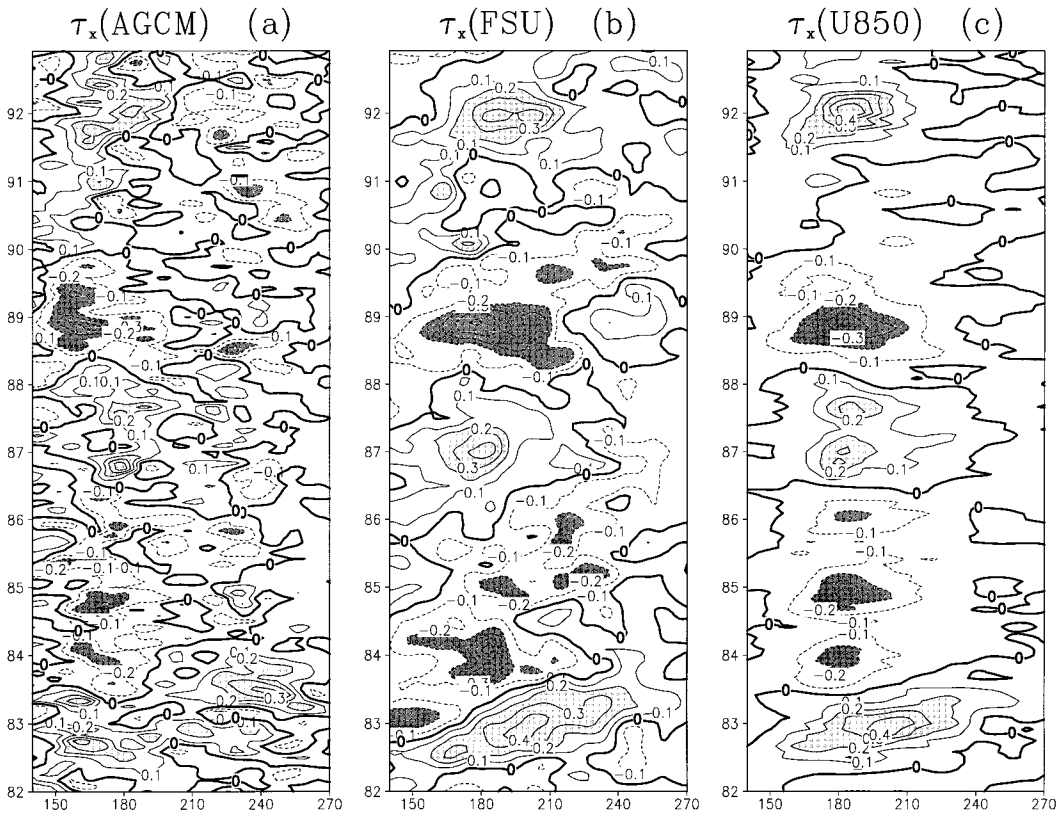

FIG. 3. Time–longitude cross section of the zonal wind stress anomaly along the equator: (a) AGCM surface stress, (b) FSU data, and (c) AGCM zonal wind converted to zonal surface stress. Contour interval 0.1 dyn cm^{-2}.

vations, it is worthwhile to note the potential advantage that this CGCM has over the more economical ICM or HCM approach. The model presented here predicts the global atmospheric circulation, rainfall, and land surface boundary conditions that makes predictions of the remote response to tropical Pacific SSTA possible. In order to predict the remote response with the ICM and HCM some sort of two-tiered approach with a physically sophisticated AGCM is required.

The procedure for calculating the surface stress from the 850-mb zonal winds uses a linear least squares fit between the AGCM 850-mb zonal wind and the FSU observed surface stress. The least squares fit defines the coefficients α and β such that

$$\tau_x = \alpha + \beta U_{850},$$

where τ_x is the zonal wind stress calculated from the 850-mb zonal wind. The coefficients α and β are functions of latitude, longitude, and month of the year, so that the annual cycle is included in the formulation for zonal wind stress. Thirty years (1964–93) of FSU data are used in calculating the least squares fit that gives 12 values of α and β for each AGCM grid point.

Figures 3a and 3b show time–longitude cross sections of the zonal wind stress anomaly (mean annual cycle removed) along the equator in the Pacific calculated from the AGCM forced with prescribed SST and the FSU analysis. In comparing the two wind stress fields, some problems with the AGCM wind stress anomalies are apparent. The AGCM anomaly is about a factor of 2 smaller than the FSU anomaly. The AGCM anomaly is too narrowly confined to the western extreme of the Pacific basin. Moreover, the weakening of the westerly anomaly during the Northern Hemisphere spring season leads to cold SSTA that serves to interrupt the warm ENSO events along the equator (Huang and Schneider 1995).

Figure 3c shows the zonal wind stress calculated from the 850-mb zonal wind, hereafter referred to as the statistically corrected zonal wind stress. In general the wind stress calculated from the AGCM 850-mb zonal wind is smoother than both the AGCM surface stress and the FSU data. There is a tendency for the statistically corrected zonal wind stress anomaly to be shifted to the east of both the FSU data and the surface wind stress anomaly. There are also some important differences in the details of the individual easterly and westerly anomaly events. For example, in the statistically corrected zonal wind stress anomaly, there is a second westerly maximum in late 1987 that is nearly absent in the FSU data. In the FSU data, there is a strong easterly anomaly in early 1984 and a somewhat weaker anomaly in early

1985. The relative strength of the easterly anomalies in 1984 and 1985 is reversed in the statistically corrected zonal wind stress.

The horizontal structure of a composite wind stress anomaly for the three wind stress fields is presented in Figs. 4a–c. The composite is calculated by taking the averaged anomaly for December–February 1965/66, 1972/73, 1982/83, 1986/87, and 1991/92. The most outstanding difference among the three composites is the degree of organization of the westerly anomalies. The AGCM surface wind stress is dominated by northerly flow along the equator turning to the west in the Southern Hemisphere with the maximum westerly anomaly at 5°S. The FSU data also has a strong northerly component along the equator but a westerly anomaly is still apparent. In the statistically corrected wind stress data, the northerly component is weaker as the anomaly is dominated by westerly flow on both sides of the equator.

There are features in the FSU and AGCM surface wind stress composite anomaly that are absent from the statistically corrected wind stress composite anomaly. For example, the northeasterly anomaly in the eastern Pacific and the equatorward flow in the south central Pacific are missing. The anomaly in the statistically corrected wind stress is smoother and more zonally oriented than either the FSU or the AGCM surface wind stress anomaly. In terms of simulating ENSO with this ocean model, the statistically corrected zonal wind stress does better at simulating the slow ENSO mode; however, it does not capture many of the observed features in the FSU data that are simulated by the AGCM surface stress.

A straightforward way to objectively determine which of these three wind stress anomaly products is best for coupling with our ocean model is to force the ocean model with these wind stress fields. In three parallel experiments we used the anomaly fields in Figs. 3a–c superimposed on the same wind stress climatology to force the ocean model. The monthly mean climatological wind stress was calculated from the FSU data in all three experiments.

Figures 5a–d show the simulated SSTA along the equator for the three experiments along with the Reynolds (1988) observed anomaly. All three simulations capture the observed interannual variability with varying degrees of fidelity. Temporal correlations and root mean square errors (see Kirtman and Schneider 1996) calculated over the complete record 1964–94 indicate that the AGCM surface wind stress gives the poorest simulation and that the AGCM statistically corrected wind stress gives a better simulation of the interannual variability than the FSU data. All three simulations fail to capture the strength of the oscillations specifically in the eastern Pacific, although the simulation in the east becomes progressively better in going from Figs. 5a to 5c. In the AGCM surface wind stress simulation, there are cold interruptions during both the 1983 and 1987 warm events. These interruptions are linked to a southward shift of the wind stress anomaly that is similar to the composite shown in Fig. 4a. Huang and Schneider (1995) have shown that this southward shift of the wind stress anomaly is connected to an erroneous southward shift of the AGCM climatological intertropical convergence zone (ITCZ).

The differences in the individual ENSO events are important, particularly if the simulations are used as initial conditions for coupled forecasts. For example, during the second half of 1987, the FSU simulation gives near normal SST, whereas both Figs. 5a and 5b indicate a secondary warming as in the observations although weaker. Coupled forecasts initialized with the FSU simulation in middle to late 1987 fail to capture warm SSTA that persists through January 1988 in the observations. The FSU simulation also has a tendency to produce a cooling trend about 3 months too early in the eastern Pacific for the 1988 cold event. Both the FSU and the statistically corrected wind stress simulation have relatively cold temperatures in the latter half of 1983 that are too strong compared to the observations and too weak in 1984–85.

A composite SSTA calculated in the same way as in Figs. 4a–c is shown in Figs. 6a–d. All three simulation composites are weak in the eastern Pacific, and the AGCM surface stress yields the weakest response. There is a local maximum in the central Pacific centered around 165°W in the simulations that is absent from the observations. The meridional scale of the simulated anomaly is also severely truncated in comparison with the observations. While it is clear that the AGCM statistically corrected wind stress gives a better simulation of the SSTA than the AGCM surface stress, neither the FSU nor the statistically corrected wind stress simulation gives sufficiently accurate initial conditions for coupled prediction.

As noted above, the training period for the coefficients α and β were determined from the FSU data from 1964–93. We have also tested the statistically corrected wind stress on an independent time period (1949–63). The uncoupled AGCM was forced with observed SST from 1949–63, and the statistically corrected wind stress was calculated using the original α and β. The statistically corrected wind stress was then used to force the uncoupled ocean model for the period of 1949–63. The improvements in the SSTA simulation were similar to those noted above and are not shown here. However, it should be noted that the training period for the statistically corrected wind stress and the hindcast period in which the verifications are made are coincident.

4. Initial conditions

In the previous section we showed that, in many ways, the zonal wind stress calculated from the AGCM 850-mb wind produces an SSTA simulation superior to both the AGCM surface wind stress and the FSU wind

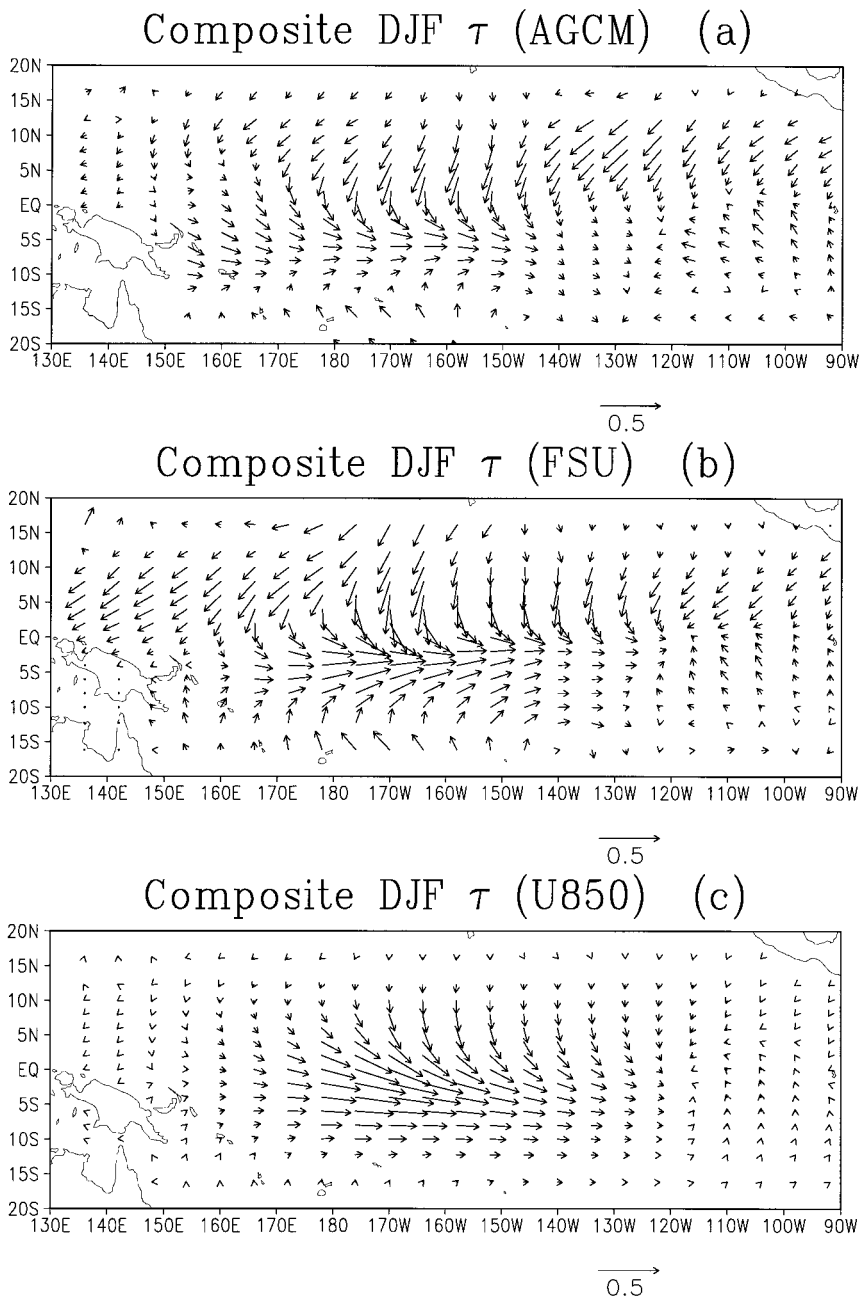

FIG. 4. Composite wind stress anomaly vectors (DJF 1965/66, 1972/73, 1982/83, 1986/87, and 1991/92): (a) AGCM surface stress, (b) FSU data, and (c) AGCM zonal wind converted to zonal surface stress.

stress. However, in terms of coupled prediction, all three simulations should be improved in order to produce initial conditions for coupled forecasts. For example, in January 1988, the Reynolds data indicate that the SST are nearly a degree warmer than normal (see Fig. 5d), whereas the statistically corrected wind stress simulation gives only a very small region near the date line where SST are above normal (see Fig. 5c). The response to FSU forcing in January 1988 is even worse (see Fig 5b). When using either the statistically corrected wind stress or the FSU wind stress simulation as an initial condition for a coupled forecast, the prediction skill, as measured by the Nino-3 SSTA correlations and rmse, starts off low and then deteriorates.

Motivated by the need to generate better ocean initial conditions without necessarily assimilating subsurface ocean data, Kirtman and Schneider (1996) developed an iterative wind stress initialization procedure. The

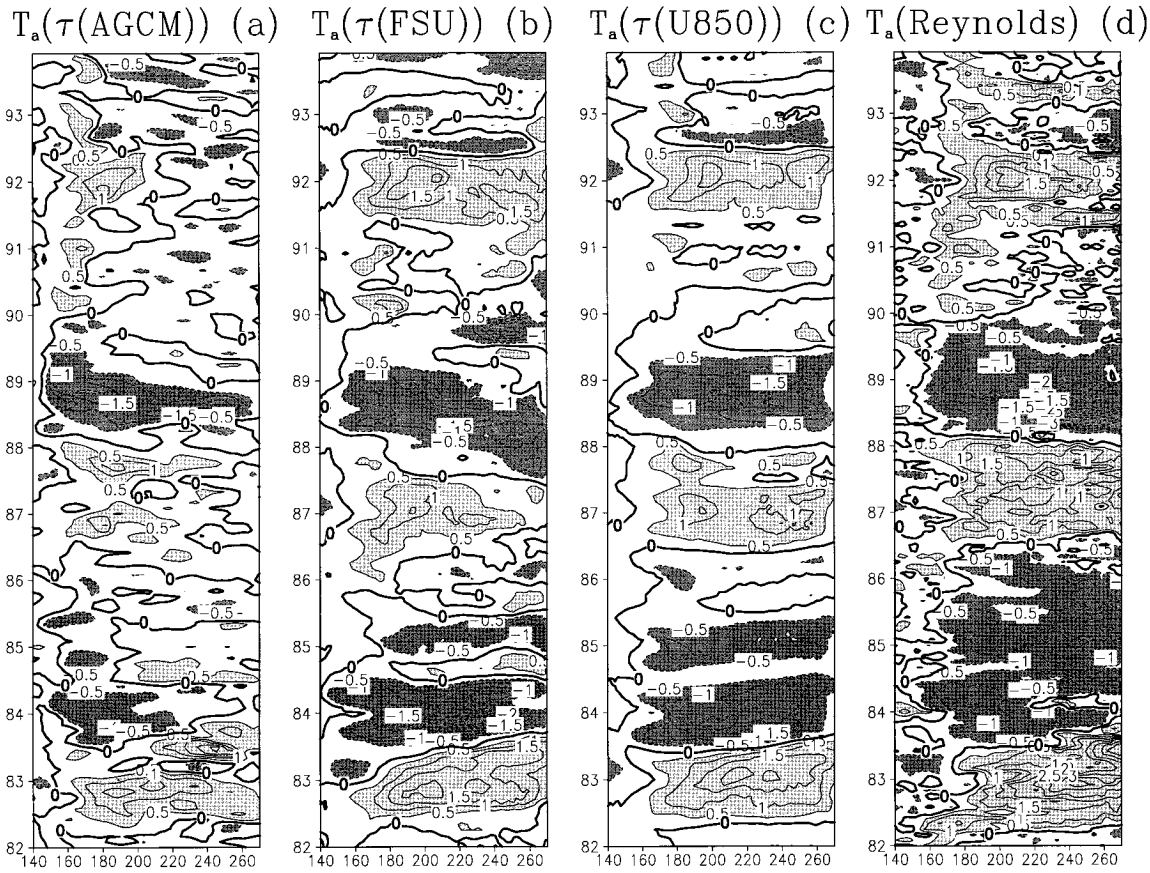

FIG. 5. Time–longitude cross section of SSTA along the equator: (a) OGCM forced by AGCM wind stress, (b) OGCM forced by FSU wind stress, (c) OGCM forced by AGCM 850-mb zonal wind converted into zonal surface stress, and (d) Reynolds analysis.

wind stress is modified to correct the simulated SSTA error. A linear adjustment was applied that was local in both space and time, where for each 1 K of SSTA simulation error the zonal wind stress anomaly was adjusted by 0.1 dyn cm^{-2}. The iteration procedure is to run the OGCM, adjust the zonal wind stress based on the SSTA error, and then repeat the process. The final product is a better ocean simulation as measured by the SSTA correlation and the rmse, and possibly a better zonal wind stress anomaly.

There are large spatial and temporal scales associated with the simulated SSTA errors, which, by definition of the iteration procedure, translate into wind stress differences among the iterates that are of the same spatial and temporal scales. Figure 7 shows the modification to the westerly zonal wind stress anomaly composite shown in Fig. 4 due to the iteration procedure. The zeroth iterate or the first guess in the iteration procedure is taken from the statistically corrected zonal wind stress. Given the similarities between Fig. 4c and Fig. 7a, the changes in the zonal wind stress are modest. In Fig. 7b only the difference in the zonal wind stress is shown as the iteration procedure does not modify the meridional wind stress. The dominant difference between the zonal wind stress before and after the iteration procedure is a large-scale eastward shift of the anomaly. The largest changes are just to the north and south of the equator in the eastern Pacific, where the iteration procedure is attempting to compensate for the truncated meridional scale seen in the ocean simulation of Fig 6.

Figure 8 shows the changes in the simulated warm SSTA composite associated with the statistically corrected wind stress before and after the iteration is applied. Consistent with the changes in the zonal wind stress anomaly, the SSTA is reduced in the central Pacific and enhanced in the eastern Pacific. The SSTA is increased just to the north and south of the equator, which reflects some meridional broadening of the simulated SSTA. In the far eastern Pacific along the equator the SSTA is also increased by as much as 0.5°C. Kirtman and Schneider (1996) calculated the Nino-3 SSTA correlation coefficient over a 30-yr simulation with the ocean model and found that the correlation increases from 0.77 before the iteration to 0.93 after the iteration. The rmse of Nino-3 SSTA was reduced from 0.57° to 0.34°C.

Given that the modification to the zonal wind stress anomaly depends on the ocean model simulation, the iteration procedure may be introducing errors into the zonal wind stress that compensate for errors in the ocean

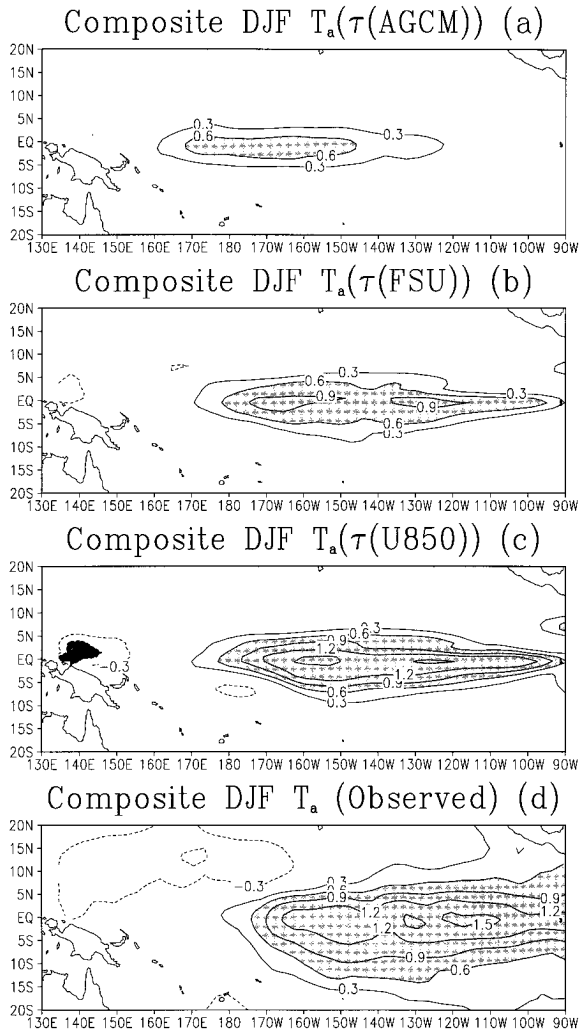

FIG. 6. Composite SSTA (DJF 1965/66, 1972/73, 1982/83, 1986/87, and 1991/92): (a) OGCM forced by AGCM surface stress, (b) OGCM forced by FSU data, (c) OGCM forced AGCM zonal wind converted to zonal surface stress, and (d) Reynolds analysis.

model. As a consequence, it is possible that errors have been introduced into the zonal wind stress that appear as temporally and spatially remote errors in the subsurface heat content. Kirtman and Schneider (1996) also considered the simulation of the subsurface heat content along the equator and found that the iteration procedure only introduces very modest improvements in the subsurface heat content over the verification period. However, the best indication of the utility of the iteration procedure is through verifying coupled prediction experiments.

5. Coupled forecast results

We have completed a set of 78 hindcast predictions for the period 1965–94 using the dynamical ocean–land–atmosphere general circulation model described in the above sections. A hindcast was initialized for each January, April, July, and October of 1965, 1966, 1970, 1972–75, 1982–84, 1986–89, and 1991, yielding 60 hindcasts. An additional 18 hindcasts initialized January and July 1977–81, 1985, 1990, 1992, and 1993 were made, so as to sample 17 consecutive years and assess the skill in making experimental forecasts without subjectively selecting individual years. Each hindcast was run for 18 months. The ocean initial conditions for all of these predictions were taken from an uncoupled simulation in which the 850-mb zonal wind was converted into a surface stress and then the iterative wind stress procedure was applied so that both the ocean and atmosphere models are close to equilibrium with the wind stress anomaly and the SSTA, respectively.

To verify the hindcasts of SSTA initialized prior to 1982, we used SST provided by C. K. Folland of the United Kingdom Meteorological Office. After 1982 we used the blended analysis of Reynolds (1988) for verification.

a. Systematic error

One of the main differences between the prediction system presented here and that used by NCEP is in the procedure for developing initial conditions. The experience at NCEP is that the ocean data assimilation system yields better forecasts, but the forecasts also have larger systematic errors. The experience at NCEP identifies both the importance of ocean data assimilation in seasonal to interannual forecasting and the need for ocean model development designed to reduce the systematic errors; in fact, the two problems are coupled and need to be addressed as such. In some sense, the iterative wind stress procedure presented here is a compromise between using ocean data assimilation and reducing the systematic errors of the forecasts. Typically, when the forecast skill is evaluated in the Nino-3 region, the systematic error is removed a posteriori. However, given the highly nonlinear nature of the remote response to tropical forcing, the systematic error will impact the remote forecast in such a way that it cannot be removed in this linear fashion. One of the advantages of the prediction system presented here is that the systematic error is relatively small compared to other similar coupled prediction systems.

The systematic error for the January predictions, for example, is defined as the mean of the anomaly predictions initialized in January. Since each prediction is 18 months in duration, there are 18 months of systematic error. The systematic error is defined as

$$T_{\text{sys}} = \frac{1}{N}\sum_{j=1}^{N}(T_p - T_c),$$

where, in this example, the summation is over forecasts initialized in January and N is the number of forecasts initialized in January. The systematic error is defined in the same way for the forecasts initialized in April,

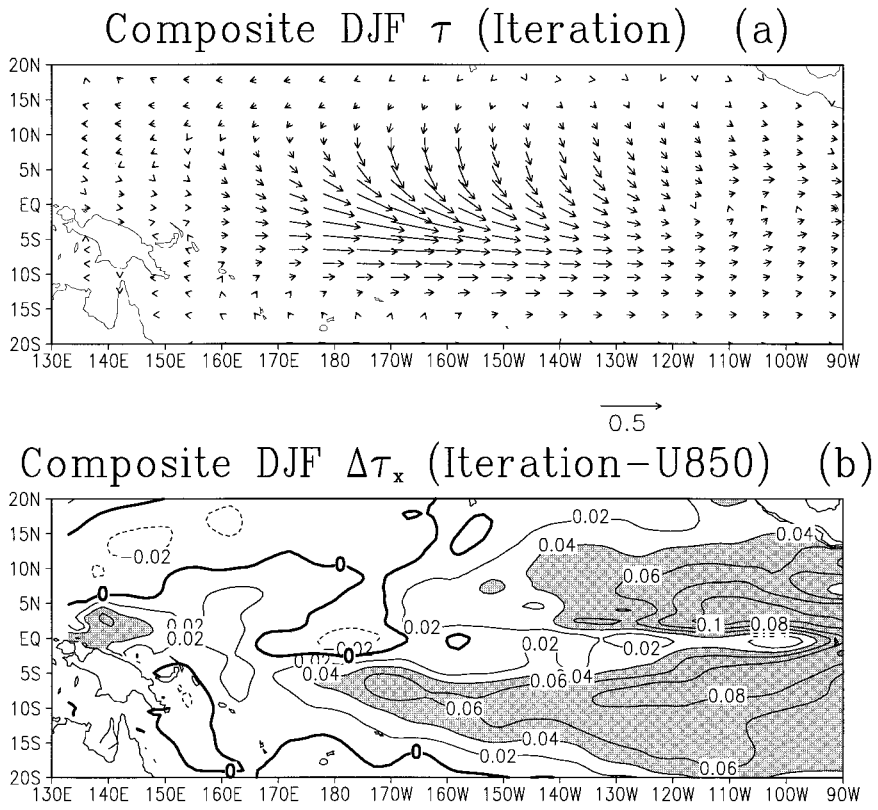

FIG. 7. Composite wind stress anomaly (DJF 1965/66, 1972/73, 1982/83, 1986/87, and 1991/92): (a) vectors after one iteration and (b) the change in the zonal wind stress anomaly due to the iteration. Contour interval 0.01 dyn cm^{-2}.

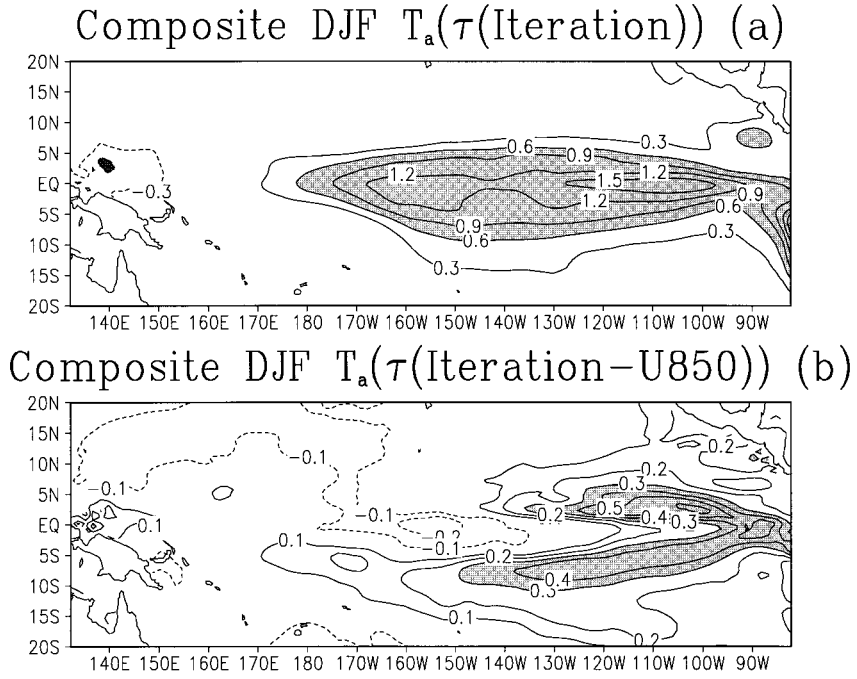

FIG. 8. Composite SSTA (DJF 1965/66, 1972/73, 1982/83, 1986/87, and 1991/92): (a) after iteration (contour interval 0.3°C) and (b) the change due to the iteration (contour interval 0.1°C).

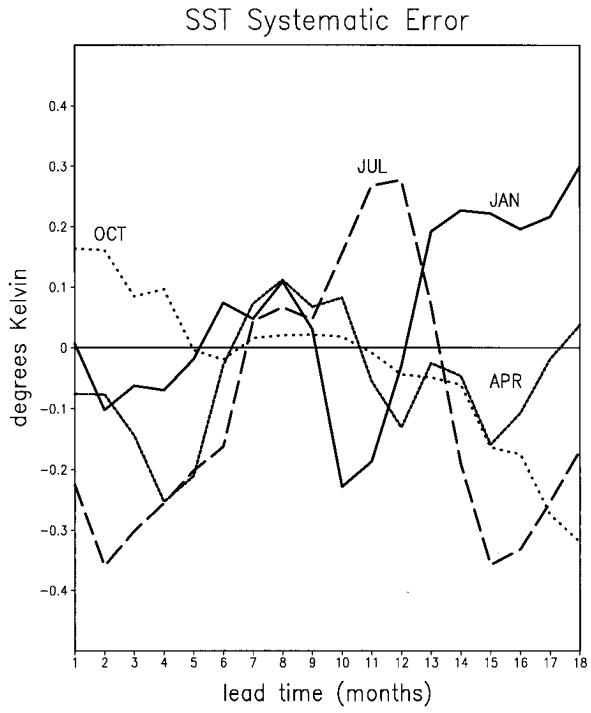

FIG. 9. Evolution of the Nino-3 SSTA systematic error. The solid curve denotes the January forecasts, the short dashed curve denotes the April forecasts, the long dashed curve denotes the July forecasts, and the dotted curve denotes the October forecasts.

July, and October. So that comparisons among all four initial months are possible, the systematic error is calculated over the initial 15-yr sample (1965, 1966, 1970, 1972–75, 1982–84, 1986–89, and 1991). The systematic error for the January and July cases only changes slightly with the inclusion of the additional 9 years.

Figure 9 shows the evolution of the Nino-3 (5°S–5°N,150°–90°W) systematic error of SST for the January, April, July, and October forecasts. For all initial months the overall systematic error is small and the initial bias is about the same as the bias for any lead time, suggesting that there is little initial shock in the forecasts due to an imbalance of the initial conditions and the ocean model.

Considering the equatorial Pacific region as a whole, the largest systematic errors occur during the 10th month (October) of the January forecasts, the 4th month (July) of the April forecasts, the 8th month (February) of the July forecasts, and the 18th month (March) of the October forecasts. Figure 10 shows the horizontal structure of these errors. For all four sets of initial conditions and all lead times, there are fairly large errors along the eastern boundary that are negative for all lead times. The January, April, and October forecasts have their largest cold errors in the eastern Pacific with a sizable region where the absolute error is greater than 0.6°C. In contrast, the July forecasts have their largest errors in the west-central Pacific. This error in the July forecasts is most likely associated with the fact that the wind stress is systematically shifted too far to the west with too strong an SST response in this region. Unfortunately, this SST error also has an associated precipitation (convective heating) error, producing an extratropical circulation error that potentially limits the predictability in the extratropics.

b. Forecast skill

The 18-month evolution of the SSTA in the Nino-3 region for all 78 hindcasts is shown in Fig. 11. The systematic error in the predicted SSTA has been removed and the observed Nino-3 SSTA is indicated by the bold solid line. It should be noted that the statistical wind stress correction procedure was derived with FSU data for the period 1964–94 and the prediction experiments presented here are dependent on the FSU observations. However, the uncoupled performance of the 850-mb wind stress correction was tested on an independent period (1948–63) and found to give similar improvements over the AGCM surface stress (see Kirtman and Schneider 1996). For the most part, the predictions track the observed anomalies for the first 12 months, although there are some notable exceptions. The forecasts initialized in January 1974, January 1989, and July 1988 have relatively cold initial states and 6–12 months later produce erroneous warm anomalies when the observed SSTA was returning to near normal conditions. There are similar problems, but with warm initial states, for the forecasts initialized in January 1966 and January 1970.

The Nino-3 SSTA correlation and root mean square error (rmse) is shown in Fig. 12. In addition to the skill of the COLA model, the skill of two other prediction systems (NCEP and ZC) is also shown. The skill scores for the other prediction systems were provided by M. Ji (1995, personal communication) and S. Zebiak (1995, personal communication), respectively. It should be noted that the verification of the other prediction systems includes different initial times and different sample sizes. The NCEP forecasts were initialized each month from October 1983 to February 1993. The ZC predictions are also monthly and are verified for January 1972–December 1992. Because the verification period and the sample sizes of the three prediction systems differ, the skill scores cannot be quantitatively compared here. Only a qualitative comparison is possible. The intention here is not to identify the best prediction system with this metric, but to demonstrate the rapid progress and the state-of-the-art in forecasting Nino-3 temperatures.

With these simple metrics, all the various prediction systems are doing a fairly reasonable job of forecasting Nino-3 SSTA. The character of the skill scores associated with the various forecasting approaches, however, varies. The CGCM methods (COLA and NCEP) are comparable, with the highest correlations during the ear-

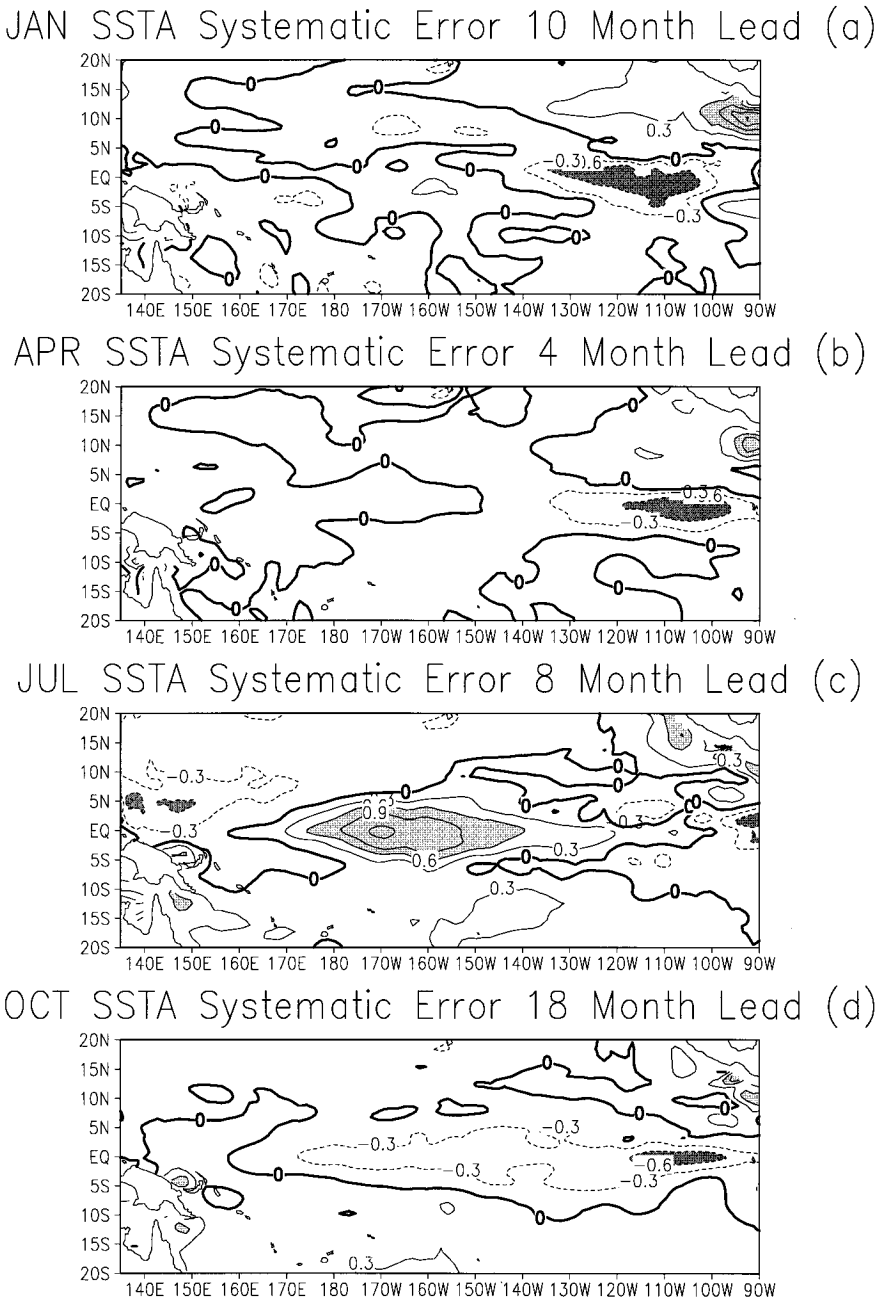

FIG. 10. Horizontal structure of the systematic error. (a) Forecasts initialized in January for lead times of 10 months, (b) forecasts initialized in April with lead times of 4 months, (c) forecasts initialized in July with lead time of 8 months, and (d) forecasts initialized in October with lead times of 18 months.

liest part of the forecast period. The skill of CGCM methods also improves significantly with the inclusion of statistical corrections to the surface wind stress forcing. The ICM approach, such as the ZC model, loses skill much less rapidly than the CGCM approach but has initial skill scores that are somewhat lower than the CGCM systems. The most recent results with the ZC model incorporate an initialization scheme that yields remarkably good skill scores out to 20 months (Chen et al. 1995).

The three curves for the COLA anomaly coupled prediction system show improvements over the course of approximately one calendar year. The earliest version of the model (COLA1) did not apply a 30-day running mean to the anomalies (SST and wind stress), did not use the statistically corrected wind stress correction, and

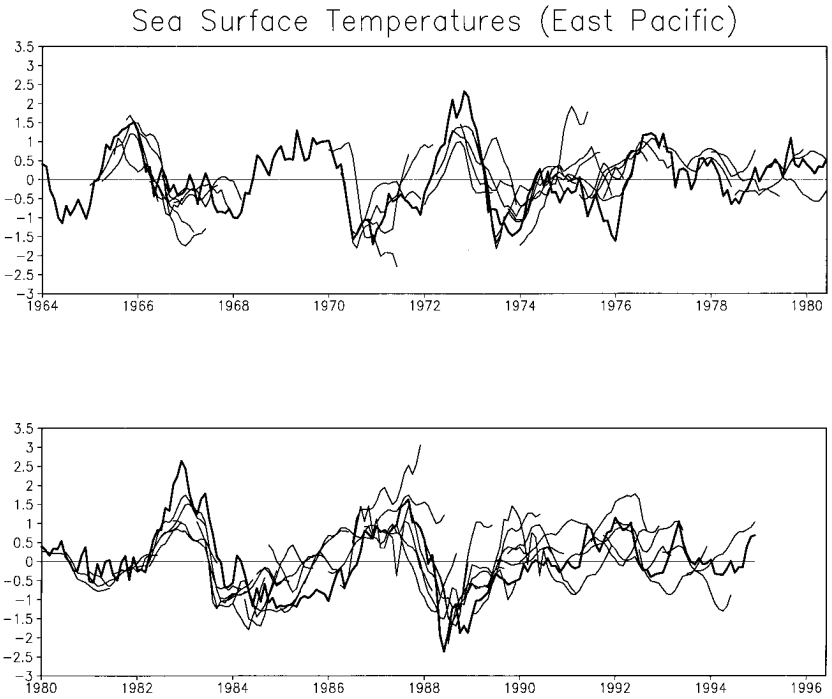

FIG. 11. Evolution of Nino-3 SSTA for all 78 forecasts and the observed SSTA. The thin curves denote the forecasts and the thick curves are for the observed SSTA.

did not use the iterative wind stress assimilation. In these early prediction experiments, the ocean initial conditions were taken from an uncoupled ocean model simulation with prescribed ECMWF wind stress forcing. The second generation of the prediction system (COLA2) incorporated a statistically corrected wind stress that omitted the annual cycle (see Huang and Shukla 1997; Kirtman et al. 1994) and the 30-day running mean was applied. The third pair of curves (COLA3) gives the correlation and rmse for the version of the COLA model described here. The correlations (rmse) have steadily increased (decreased) with changing versions of the model, where, with the most recent version of the model, the correlation remains above 0.6 for lead times up to 12 months.

In controlled experiments, we have examined the sensitivity of a subset of the prediction experiments to the statistically corrected wind stress and the initial conditions that arise for the wind stress iteration. The bulk of the reduction in the error and the increased correlation seen in Fig. 12 is due to the statistically corrected wind stress in improving both ocean initial conditions and the wind stress forcing that is felt by the ocean component of the coupled model. The iteration wind stress initial conditions also improve the correlation and reduce the error particularly in the early part of the forecast period.

From 1977 to 1993 we have made a hindcast for each January and July giving a total of 34 predictions. The Nino-3 correlation and rmse was recomputed including only these 34 cases and was found to be qualitatively similar to the curves shown in Fig. 12 with Nino-3 correlations greater that 0.6 for lead time of up to 12 months. This indicates that the prediction system is potentially useful for operational ENSO forecasting.

6. Composite warm events

Composites of the predicted SSTA, circulation, and rainfall identify those features in the hindcasts that are well simulated and those that are poorly simulated. Similar to the NCEP forecasts, the COLA predictions verify somewhat better in the central Pacific than in the eastern Pacific. This is primarily due to the fact that the AGCM wind stress response to the observed SSTA is strongest in the western and west-central Pacific, and the response farther to the east is quite weak and often of the wrong sign. The strong response in the central Pacific can be seen in Fig. 13, where the hindcast and observed SSTA for composite warm (DJF 1965/66, DJF 1972/73, DJF 1982/83, and DJF 1986/87) events is plotted. For all the composites we show the forecasts initialized in July, so the figures plotted are for lead times of 6–8 months.

The SSTA, zonal wind stress, sea level pressure, and precipitation composites show that the predictions contain many of the basic features of ENSO: warm SSTA in the eastern and central tropical Pacific with accompanying westerly zonal wind stress anomaly, nearly global-scale oscillations in the sea level pressure, and large-scale shifts in the ITCZ complexes. The composite predictions of the SSTA are slightly too weak and do

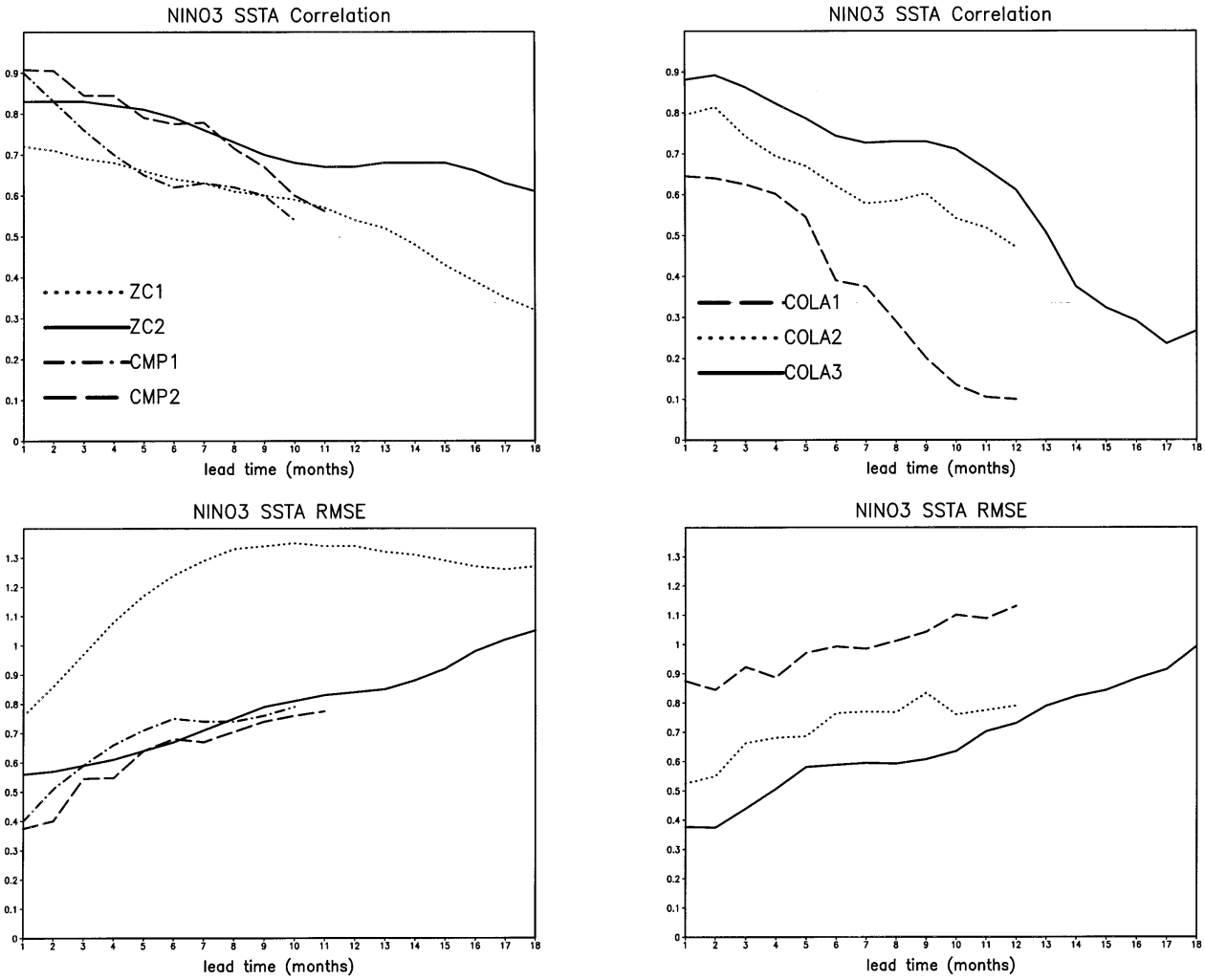

FIG. 12. Nino-3 correlation coefficient and rmse. The curves marked ZC1 and ZC2 are for the Zebiak–Cane model without and with the initialization procedure, respectively (see Chen et al. 1995). The curves marked CMP1 and CMP2 are for the NCEP coupled model project before and after the statistical correction was applied to the wind stress (Ji et al. 1994, 1995). The curves marked COLA1, COLA2, and COLA3 denote various versions of the prediction model presented here (see text for details) and the most recent version is COLA3.

a better job of capturing the amplitude and meridional extent in the central part of the basin. The predictions also capture a suggestion of the anomaly extending along the South American coast in the Nino-1 and Nino-2 regions. In the observed warm composites, there are subtropical anomalies of the opposite sign in the western Pacific. The predictions also give anomalies of the opposite sign in the western Pacific, but they are confined too close to the equator.

A clear deficiency in the predictions is in the meridional extent of the SSTA. The observed anomaly extends into the subtropics, whereas the predicted SSTA is confined to the region between 5°S and 5°N. Simulating the correct meridional extent may be particularly important in terms of capturing the extratropical atmospheric response, as has been pointed out by Held and Kang (1987) and Held et al. (1989), who find that the extratropical response depends on the extension of the SSTA into the subtropics.

The lack of an extension into the subtropics is due to problems in both the AGCM wind stress and errors in the ocean model. In uncoupled simulations with this ocean model, the meridional extent of the SSTA is also too narrow, and even the statistically corrected wind stress does not extend far enough off the equator (see Figs. 4 and 6). In the coupled prediction model, these two problems can reinforce each other, which leads to further confinement of the predicted anomaly. In other words, a narrow band of SSTA leads to a narrowing of the zonal wind stress anomaly, which then leads to even further narrowing of the SSTA. The equatorial confinement of the wind stress anomaly can be seen in Fig. 14, which shows the warm event zonal wind stress anomaly composite. The iteration zonal wind stress composite is

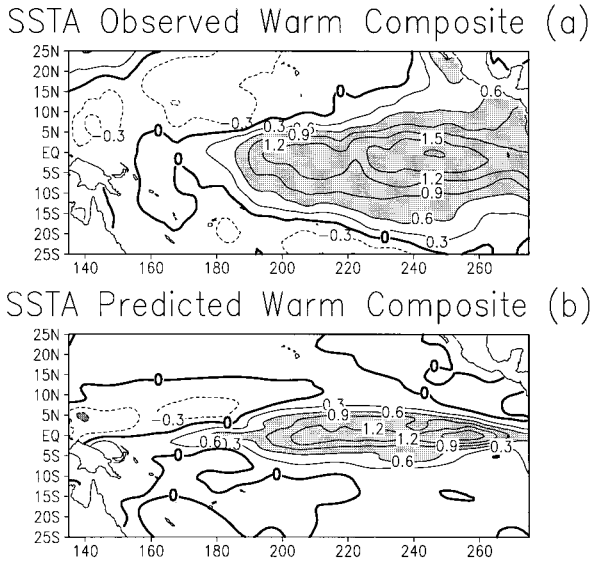

FIG. 13. Horizontal structure of the (a) observed and (b) predicted SSTA warm composite (DJF 1965/66, DJF 1972/73, DJF 1982/83, DJF 1986/87, DJF 1991/92).

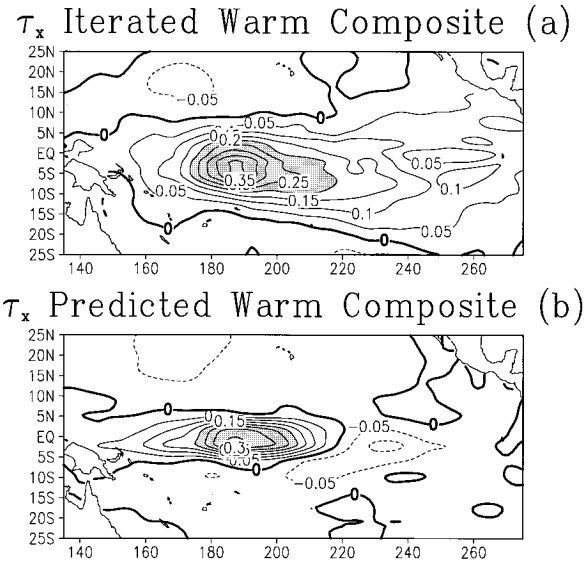

FIG. 14. Horizontal structure of the (a) iteration and (b) predicted zonal wind stress anomaly warm composite (DJF 1965/66, DJF 1972/73, DJF 1982/83, DJF 1986/87, DJF 1991/92).

also shown for comparison. The anomaly is meridionally truncated in comparison with the iterated zonal wind stress. There is also the appearance of a weak anomaly of the opposite sign in the eastern Pacific that inhibits the growth of the SSTA in the east. The westerly anomaly extends farther to the west than the assimilated wind stress in a narrow region along the equator. This is consistent with the erroneous warm tongue in the predicted SSTA and the July systematic error. In multidecade integrations of this anomaly coupled model, the equatorial confinement and westward expansion of the warm and cold events becomes even more enhanced.

The weak wind stress anomaly is consistent with the sea level pressure anomaly shown in Fig. 15. For comparison, we show the sea level pressure composite anomaly calculated from a long integration (1948–95) of the AGCM with observed SST. The simulation of the uncoupled Southern Oscillation index (SOI) is realistic and the predictions capture the major oscillations of the simulated SOI (not shown). The predictions also capture the broad horizontal structure of the east–west contrast in the Southern Oscillation; however, the zonal gradient of the predicted sea level pressure anomaly is weak in comparison with the uncoupled simulation of the sea level pressure anomaly. Again, the node of the sea level pressure anomaly is shifted westward in the case of the warm events similar to the wind stress anomaly and the SSTA.

The warm composite precipitation anomaly is shown in Fig. 16. The uncoupled simulation with observed SST provides a homogeneous precipitation record for comparison. The uncoupled AGCM has a reasonable simulation of tropical and subtropical precipitation anomalies, and it provides a useful measure of what could be simulated from the anomaly coupled model if the predicted SSTA were perfect. In the tropical Pacific, the anomaly coupled model has predicted the basic features of the simulation, with reduced rainfall throughout most of the Pacific and enhanced rainfall in the warm composite. There are anomalies in the subtropical Pacific and the remote parts of the Tropics for which the simulation and the predictions are consistent. For example, the uncoupled simulation and the prediction give reduced subtropical rainfall straddling the enhanced rainfall. Rainfall anomalies over Australia, tropical Africa, and Brazil also appear to be potentially predictable.

As expected, the uncoupled simulated rainfall anomalies are somewhat stronger than the predicted anomalies. The predicted composite rainfall anomaly is also shifted too far to the west much like the other composites. The extratropical response is sensitive to these structural and amplitude differences. We have formed composites of the 200-mb height anomalies and compared them with the uncoupled simulations (not shown). In the Tropics, the agreement is reasonable: the uncoupled simulation and the predictions produce warming of the tropical troposphere with increased geopotential height. However, there is little agreement between the simulation and the predictions in the extratropics. Part of the problem is that the AGCM response to tropical heating anomalies is weak and larger ensembles are required to obtain robust extratropical signals.

7. Summary and concluding remarks

The prediction experiments presented here show that ENSO and ENSO-related climate anomalies in the Tropics are potentially predictable with complex ocean–

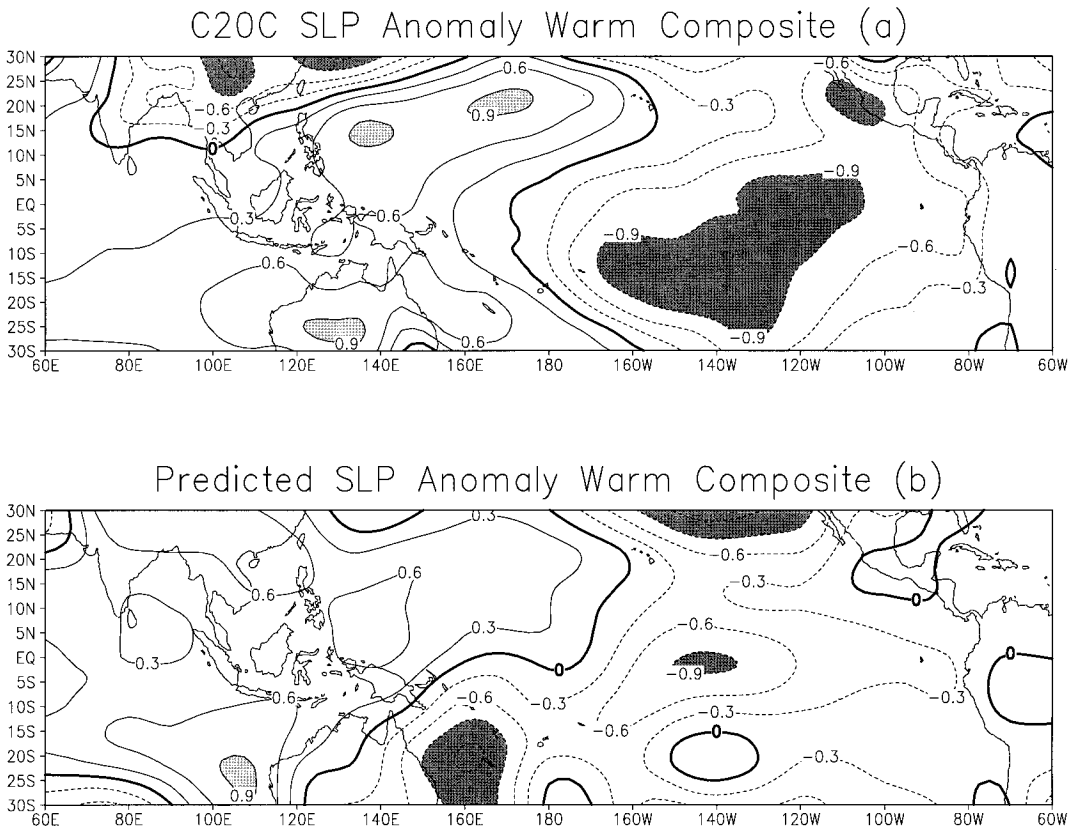

FIG. 15. Horizontal structure of the (a) AGCM uncoupled sea level pressure anomaly simulation with observed SST and (b) predicted sea level pressure anomaly warm composite (DJF 1965/66, DJF 1972/73, DJF 1982/83, DJF 1986/87, DJF 1991/92).

land–atmosphere general circulation models. However, the fact that the anomaly coupling strategy was employed and statistical corrections to the wind stress were required indicates that there is ample opportunity to improve the coupling strategy, the component models, and, ultimately, the predictions.

Long uncoupled simulations of the ocean and atmosphere component models showed errors in the simulated annual cycles of SST and wind stress that, in the directly coupled model, lead to large climate drift and weak interannual variability. Based on the performance of the uncoupled component atmosphere and ocean models, we have taken the anomaly CGCM approach for seasonal to interannual climate predictions. Following Huang and Shukla (1997) and Kirtman and Schneider (1996), we have empirically converted the 850-mb zonal winds into a zonal surface stress for prediction experiments presented here. We have also used the iterative wind stress procedure described in Kirtman and Schneider (1996) to generate ocean initial conditions. This simple iterative procedure has the advantage that the systematic error of the predictions is relatively small in comparison to sophisticated ocean data assimilation systems; however, we do not see the dramatic increase in predictive skill that is typically obtained with the assimilation of observed subsurface thermal data.

Based on 78 18-month hindcast experiments including warm, cold, and normal years, the predictions are found to have useful skill up to at least 12 months lead time as measured by the Nino-3 SSTA correlation and rmse. The skills of the two CGCM (COLA and NCEP) forecasts are comparable, and, for the early part of the forecast period, the CGCM predictions have larger correlations than the ICM approach, but the ICM approach gives better results for lead times greater than 12 months. Some of the predictions that started from cold initial states produced erroneous warm anomalies 6–12 months later when the observed SSTA was returning to near normal conditions. In extended integrations of the prediction model, fairly strong biennial oscillations are observed, suggesting that the model has a tendency to oscillate between the extreme ENSO states, which is consistent with the problems in some of the prediction experiments.

Composites of the warm and cold predicted SSTA show that the meridional structure of the anomaly is too narrow, and there is a tendency to over predict the anomaly in the central and western Pacific. Composites of

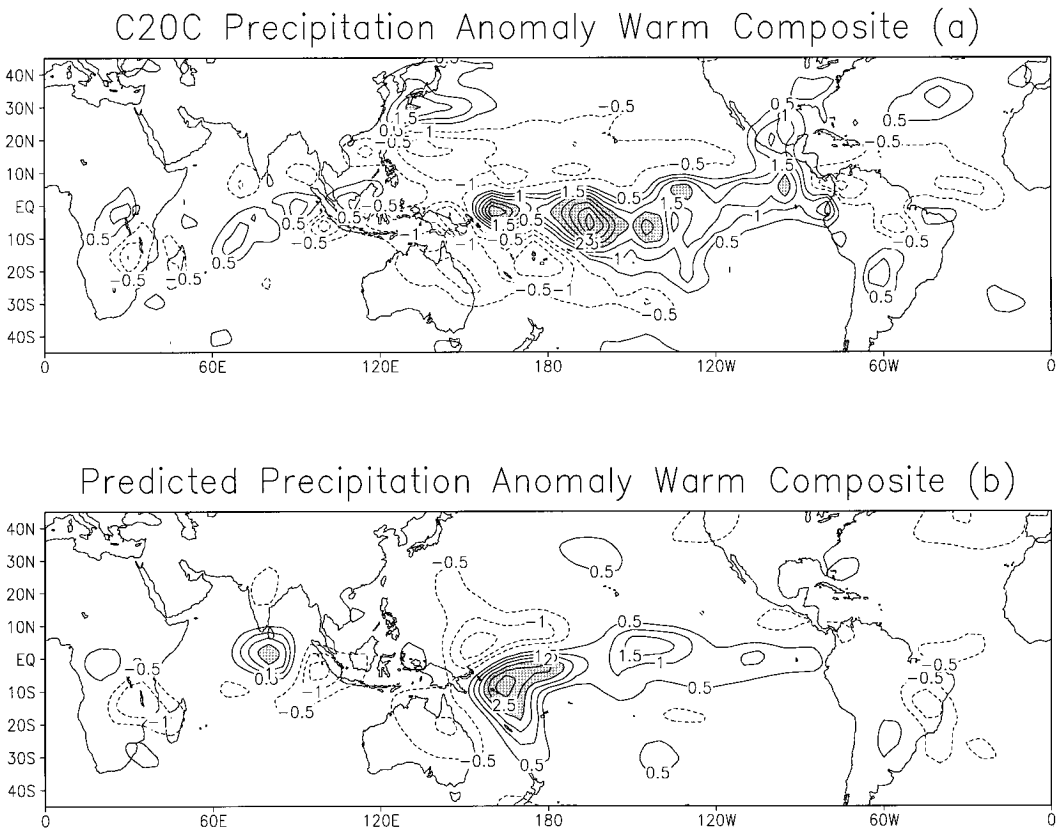

FIG. 16. Horizontal structure of the (a) AGCM uncoupled precipitation anomaly simulation with observed SST and (b) predicted precipitation anomaly warm composite (DJF 1965/66, DJF 1972/73, DJF 1982/83, DJF 1986/87, DJF 1991/92).

the atmospheric response are encouraging, particularly for the rainfall anomalies in the tropical Pacific. The 200-mb extratropical height anomalies are not realistic, indicating that larger ensembles are required and improvements to the atmospheric model must also be made.

The skill of earlier versions of the model without the statistically corrected wind stress or the iterative wind stress assimilation was also briefly discussed. Some sensitivity experiments were also performed that were intended to isolate the relative effects of the statistically corrected wind stress and the iterative wind stress assimilation. In general, the statistically corrected wind stress was shown to give the greatest improvement in the forecasts and the iterative wind stress assimilation improved the forecasts, particularly for short lead times.

While the results presented here are encouraging, there are a number of things that need to be improved with the model. The most serious problem is with the horizontal structure of the uncoupled and coupled SSTA. The parameterized heat flux, which acts to damp the SSTA, is a particularly bad formulation off the equator and possibly contributes to this problem. The heat flux into the ocean model needs to be changed to include anomalies from the atmospheric model. Refinements to the vertical mixing parameterization in the ocean model will also lead to improvements in the meridional structure of the SSTA. There are active research efforts at COLA designed to improve the AGCM tropical boundary layer and the extratropical response to observed SSTA. We need to consider ensemble prediction in order to capture the extratropical response, and we need to sample a larger set of initial conditions in our skill assessment. We are actively pursuing a number of different approaches to ocean data assimilation that are designed to improve the ocean model, the ocean model simulation, and the coupled forecasts, without introducing additional systematic error.

Acknowledgments. This research is part of a larger effort at COLA to study the predictability of the coupled system. Members (J. Kinter, L. Marx, D. DeWitt, and M. Fennessy) of this group have provided invaluable advise. The extended integrations of the uncoupled AGCM were performed by L. Marx. M. Ji, and S. Zebiak provided the skill scores for the NCEP and ZC models, and we are grateful for their support and comments. We are also thankful to R. Reynolds and C. K. Folland for providing the SST data. L. Kikas assisted in archiving and managing the data. Anonymous re-

viewers' comments were helpful in improving this manuscript. A large amount of computer time for this project was provided though NOAA's Office of Global Programs, and we are very grateful to K. Mooney for providing this computer time. This work was supported under NOAA Grants NA26-GPO149 and NA46-GPO217, and NSF Grant ATM-93021354.

REFERENCES

Balmaseda, M. A., Anderson, D. L. T., and M. K. Davey, 1994: ENSO prediction using a dynamical ocean coupled to a statistical atmosphere. *Tellus,* **46A,** 497–511.

Barnett, T. P., M. Latif, N. Graham, M. Flugel, S. Pazan, and W. White, 1993: ENSO and ENSO-related predictability. Part I: Prediction of equatorial Pacific sea surface temperature with a hybrid coupled ocean–atmosphere model. *J. Climate,* **6,** 1545–1566.

——, and Coauthors, 1994: Forecasting global ENSO-related climate anomalies. *Tellus,* **46A,** 381–397.

Barnston, A. G., and C. F. Ropelewski, 1992: Prediction of ENSO episodes using canonical correlation analysis. *J. Climate,* **5,** 1316–1345.

Blumenthal, M. B., 1991: Predictability of a coupled ocean–atmosphere model. *J. Climate,* **4,** 766–784.

Bryan, K., and L. Lewis, 1979: A water mass model of the world ocean. *J. Geophys. Res.,* **84,** 2503–2517.

Cane, M. A., and S. E. Zebiak, 1985: A theory for El Niño and the Southern Oscillation. *Science,* **228,** 1085–1087.

——, and ——, 1987: Predictions of El Niño events using a physical model. *Atmospheric and Oceanic Variability,* H. Cattle, Ed., Roy. Meteor. Soc. Press, 153–182.

——, ——, and S. C. Dolan, 1986: Experimental forecasts of El Niño. *Nature,* **321,** 827–832.

Chen, D., S. E. Zebiak, A. J. Busalacchi, and M. A. Cane, 1995: An improved procedure for El Niño forecasting. *Science,* **22,** 1699–1702.

Fennessy, M. J., and J. Shukla, 1991: A comparison of the impact of the 1982–83 and 1986–87 Pacific SST anomalies on time mean prediction of atmospheric circulation and rainfall. *J. Climate,* **4,** 407–423.

——, and Coauthors, 1994: The simulated Indian monsoon: A GCM sensitivity study. *J. Climate,* **7,** 33–43.

Gill, A. E., 1980: Some simple solution for heat induced tropical circulations. *Quart. J. Roy. Meteor. Soc.,* **106,** 447–462.

Goldenberg, S. B., and J. J. O'Brien, 1981: Time and space variability of the tropical Pacific wind stress. *Mon. Wea. Rev.,* **109,** 1190–1207.

Goswami, B. N., and J. Shukla, 1991a: Predictability of a coupled ocean–atmosphere model *J. Climate,* **4,** 1–22.

——, and ——, 1991b: Predictability and variability of a coupled ocean–atmosphere model. *J. Mar. Syst.,* **1,** 271–275.

Graham, N. E., and T. P. Barnett, 1995: ENSO and ENSO-related predictability. Part II: Northern Hemisphere 700-mb height predictions based on a hybrid coupled ENSO model. *J. Climate,* **8,** 544–549.

Harshvardhan, R. Davis, D. A. Randall, and T. G. Corsetti, 1987: A fast radiation parameterization for general circulation models. *J. Geophys. Res.,* **92,** 1009–1016.

Held, I. M., and I.-S. Kang, 1987: Barotropic models of the extratropical response to El Niño. *J. Atmos. Sci.,* **44,** 3576–3586.

——, S. W. Lyons, and S. Nigam, 1989: Transients and the extratropical response to El Niño. *J. Atmos. Sci.,* **46,** 163–174.

Helfand, H. M., J. C. Jusem, J. Pfaendtner, J. Tenenbaum, and E. Kalney, 1987: The effect of a gravity wave drag parameterization on GLA fourth-order GCM forecasts. *NWP Symp. on Short- and Medium-Range Weather Prediction,* Tokyo, Japan, World Meteorological Organization/International Union of Geophysics and Geoscience, 4–8.

Huang, B., and E. K. Schneider, 1995: The response of an ocean general circulation model to surface wind stress produced by an atmospheric general circulation model. *Mon. Wea. Rev.,* **123,** 3059–3085.

——, and J. Shukla, 1997: An examination of the AGCM simulated surface wind stress and low-level winds over the tropical Pacific Ocean. *Mon. Wea. Rev,* **125,** 985–998.

Ji, M., and A. Leetmaa, 1993: Modes of interannual tropical ocean–atmosphere interaction—A unified view. Part III: Analytical results in fully coupled cases. *J. Atmos. Sci.,* **50,** 3523–3540.

——, and A. Kumar, 1994: A multiseason climate forecast system at the National Meteorological Center. *Bull. Amer. Meteor. Soc.,* **75,** 569–577.

——, ——, and A. Leetmaa, 1994: An experimental coupled forecast system at the National Meteorological Center: Some early results. *Tellus,* **46A,** 398–418.

——, A. Leetmaa, and J. Derber, 1995: An ocean analysis system for seasonal to interannual climate studies. *Mon. Wea. Rev.,* **123,** 460–481.

——, ——, and V. E. Kousky, 1996: Coupled model predictions of ENSO during the 1980s and early 1990s at the National Centers for Environmental Prediction. *J. Climate,* **9,** 3105–3120.

Jin, F.-F., and J. D. Neelin, 1993: Modes of interannual tropical ocean–atmosphere interaction—A unified view. Part I: Numerical results. *J. Atmos. Sci.,* **50,** 3477–3503.

——, ——, and M. Ghil, 1994: El Niño on the Devil's Staircase: Annual subharmonic steps to chaos. *Science,* **264,** 70–72.

Kinter, J. L., III, J. Shukla, L. Marx, and E. K. Schneider, 1988: A simulation of winter and summer circulations with the NMC global spectral model. *J. Atmos. Sci.,* **45,** 2486–2522.

Kirtman, B. P., and E. K. Schneider, 1996: Model based estimates of equatorial Pacific wind stress. *J. Climate,* **9,** 1077–1091.

——, A. Vernekar, D. DeWitt, and J. Zhou, 1993: Impact of orographic gravity wave drag on extended range forecasts with the COLA-GCM. *Atmosphera,* **6,** 3–24.

——, B. Huang, Z. Zhu, J. Shukla, E. K. Schneider, L. Marx, D. DeWitt, M. J. Fennessy, and J. L. Kinter III, 1994: Coupled Predictions at COLA. *Proc. 19th Annual Climate Diagnostics Workshop,* College Park, MD, Center for Ocean–Land–Atmosphere Studies, 440–443.

Kleeman, R., 1993: On the dependence of hindcast skill on ocean thermodynamics in a coupled ocean–atmosphere model. *J. Climate,* **6,** 2012–2033.

——, A. M. Moore, and N. R. Smith, 1995: Assimilation of subsurface thermal data into an intermediate tropical coupled ocean–atmosphere model. *Mon. Wea. Rev.,* **123,** 3103–3113.

Kuo, H. L., 1965: On the formation and intensification of tropical cyclones through latent heat release by cumulus convection. *J. Atmos. Sci.,* **22,** 40–63.

Lacis, A. A., and J. E. Hansen, 1974: A parameterization for the absorption of solar radiation in the earth's atmosphere. *J. Atmos. Sci.,* **32,** 118–133.

Latif, M., and A. Villwock, 1990: Interannual variability as simulated in coupled ocean–atmosphere models. *J. Mar. Syst.,* **1,** 51–60.

——, A. Sterl, E. Maier–Reimer, and M. M. Junge, 1993a: Climate variability in a coupled GCM. Part I: The tropical Pacific. *J. Climate,* **6,** 5–21.

——, ——, ——, and ——, 1993b: Structure and predictability of the El Niño/Southern Oscillation phenomena in a coupled ocean–atmosphere general circulation model. *J. Climate,* **6,** 700–708.

——, T. P. Barnett, M. A. Cane, M. Flugel, N. E. Graham, H. von Storch, J.-S. Xu, and S. E. Zebiak, 1994: A review of ENSO prediction studies. *Climate Dyn.,* **9,** 167–179.

Leetmaa, A., and M. Ji, 1989: Operational hindcasting of the tropical Pacific. *Dyn. Atmos. Oceans,* **13,** 465–490.

Mechoso, C. R., and Coauthors, 1995: The seasonal cycle over the tropical Pacific in general circulation models. *Mon. Wea. Rev.,* **123,** 2825–2838.

Mellor, G. L., and T. Yamada, 1982: Development of a turbulence closure model for geophysical fluid problems. *Rev. Geophys. Space Phys.,* **20,** 851–875.

Miyakoda, K., and J. Sirutis, 1977: Comparative integrations of global spectral models with various parameterized processes of subgrid scale vertical transports. *Beitr. Phys. Atmos.,* **50,** 445–487.

Neelin, J. D., 1990: A hybrid coupled general circulation model for El Niño studies. *J. Atmos. Sci.,* **47,** 674–693.

——, and F.-F. Jin, 1993: Modes of interannual tropical ocean–atmosphere interaction—A unified view. Part II: Analytical results in the weak coupling limit. *J. Atmos. Sci.,* **50,** 3504–3522.

Pacanowski, R. C., and S. G. H. Philander, 1981: Parameterization of the vertical mixing in numerical models of tropical oceans. *J. Phys. Oceanogr.,* **11,** 1443–1451.

——, K. Dixon, and A. Rosati, 1993: The GFDL modular ocean model users guide, version 1.0. GFDL Ocean Group Tech. Rep. No. 2, 77 pp. [Available from GFDL/NOAA, Princeton University, Princeton, NJ 08542.]

Palmer, T. N., G. J. Shutts, and R. Swinbank, 1986: Alleviation of a systematic westerly bias in general circulation and numerical weather prediction model through an orographic gravity wave parameterization. *Quart. J. Roy. Meteor. Soc.,* **112,** 1001–1039.

Philander, S. G. H., 1990: *El Niño, La Niña, and the Southern Oscillation*. Academic Press, 293 pp.

——, and R. C. Pacanowski, 1986: A model of the seasonal cycle in the tropical Atlantic. *J. Geophys. Res.,* **91,** 14 192–14 206.

——, ——, N. C. Lau, and M. J. Nath, 1992: Simulation of ENSO with a global atmospheric GCM coupled to a high-resolution, tropical Pacific ocean GCM. *J. Climate,* **5,** 308–329.

Pierrehumbert, R. T., 1987: An essay on the parameterization of orographic gravity wave drag. Geophysics Fluid Dynamics Laboratory/NOAA/Princeton University, 32 pp. [Available from GFDL/NOAA, Princeton University, Princeton, NJ 08542.]

Reynolds, R. W., 1988: A real time global sea surface temperature analysis. *J. Climate,* **1,** 75–86.

Rosati, A., and K. Miyakoda, 1988: A general circulation model for upper ocean simulation. *J. Phys. Oceanogr.,* **18,** 1601–1626.

Schneider, E. K., and J. L. Kinter III, 1994: An examination of internally generated variability in long climate simulations. *Climate Dyn.,* **10,** 181–204.

——, B. Huang, and J. Shukla, 1995: Ocean wave dynamics and El Niño. *J. Climate,* **8,** 2415–2439.

——, Z. Zhu, B. Huang, B. Giese, B. P. Kirtman, and J. Shukla, 1997: Annual cycle and ENSO in a coupled ocean–atmosphere general circulation model. *Mon. Wea. Rev.,* **125,** 680–702.

Tiedtke, M., 1984: The effect of penetrative cumulus convection on the large-scale flow in a general circulation model. *Beitr. Phys. Atmos.,* **57,** 216–239.

Trenberth, K. E., W. G. Large, and J. G. Olson, 1990: The mean annual cycle in global ocean wind stress. *J. Phys. Oceanogr.,* **20,** 1742–1760.

Xue, Y., P. J. Sellers, J. L. Kinter III, and J. Shukla, 1991: A simple biosphere model for global climate studies. *J. Climate,* **4,** 345–364.

Zebiak, S. E., and M. A. Cane, 1987: A model of El Niño and the Southern Oscillation. *Mon. Wea. Rev.,* **115,** 2262–2278.

Zhu, Z., and E. K. Schneider, 1995: Experimental multi-season ENSO predictions with an anomaly coupled general circulation model. COLA Tech. Rep. 10, 18 pp. [Available from COLA, 4041 Powder Mill Rd., Suite 302, Calverton, MD 20705.]